



OPEN

Localized UV emitters on the surface of β -Ga₂O₃

Jesse Huso¹, Matthew D. McCluskey^{1,2✉}, Yinchuan Yu², Md Minhazul Islam³ & Farida Selim³

Monoclinic gallium oxide (β -Ga₂O₃) is attracting intense focus as a material for power electronics, thanks to its ultra-wide bandgap (4.5–4.8 eV) and ability to be easily doped *n*-type. Because the holes self-trap, the band-edge luminescence is weak; hence, β -Ga₂O₃ has not been regarded as a promising material for light emission. In this work, optical and structural imaging methods revealed the presence of localized surface defects that emit in the near-UV (3.27 eV, 380 nm) when excited by sub-bandgap light. The PL emission of these centers is extremely bright—50 times brighter than that of single-crystal ZnO, a direct-gap semiconductor that has been touted as an active material for UV devices.

Monoclinic gallium oxide (β -Ga₂O₃) is a potentially important material for power electronics applications, owing to its ultra-wide bandgap and ability to be doped *n*-type^{1–6}. In contrast to nitride semiconductors, Ga₂O₃ bulk single crystals can be grown from the melt without the need for extreme pressures. β -Ga₂O₃ (space group *C2/m*) is the thermodynamically stable phase, with **a** \perp **c**, **b** \perp **c**, and an angle of 104° between the **a** and **c** axes^{7,8}. (Hereafter, β -Ga₂O₃ is referred to as Ga₂O₃). Point defects affect properties such as electrical conductivity and the critical breakdown field⁹. Along with altering the electronic properties, defects are responsible for UV/visible emission bands in photoluminescence (PL) and cathodoluminescence (CL) experiments.

Density functional calculations indicate that the valence band is very flat, the conduction-band minimum (CBM) is at the Brillouin zone center, and the bandgap is 4.5–4.8 eV^{10–12}. A photo-generated hole in the VB will form a self-trapped hole (STH) that is localized at a specific oxygen atom^{13–15}. An electron in the CB, on the other hand, is delocalized and acts as a free electron. The intrinsic recombination of electrons with STHs results in the UV band, peaked at 3.4 eV (360 nm)^{16–18}. Because the self-trapping involves significant lattice relaxation, this emission is rather weak. Bands at lower energies, designated UV' (3.1 eV, 400 nm), blue (2.9 eV, 430 nm), and green (2.4 eV, 520 nm), are due to donor–acceptor pair transitions^{19–24}.

Annealing Ga₂O₃ in hydrogen is a potential method to passivate defects and improve material quality. Prior work has shown that hydrogen forms complexes with gallium vacancies²⁵, acceptor dopants^{26,27}, and possibly iridium²⁸. By removing compensating defect levels, hydrogen passivation may reduce ion impurity scattering and hence improve free-electron mobility. However, hydrogen reduction can cause oxide crystals to decompose. In this work, we report PL emission correlated with surface pits in hydrogenated Ga₂O₃.

Methods

In the present work, undoped β -Ga₂O₃ bulk single crystals were grown at Tamura Inc., Japan by the edge-defined film-fed growth (EFG) method. The samples were diced to 5 × 5 × 0.5 mm and annealed in hydrogen atmosphere in closed ampoule at 950 °C. X-ray diffraction (XRD) measurements of the as-grown and hydrogenated samples showed that the crystals are oriented in the (010) direction and the degree of crystallinity improved after hydrogen annealing (Supplementary Fig. S1). This result is qualitatively similar to prior work on thin films, which showed that annealing in air increases the degree of crystallinity and surface roughness²⁹. Optical transmission spectra showed a bandgap onset at 4.5 eV (Supplementary Fig. S2).

PL and PL excitation (PLE) spectra were obtained with a Horiba FL3-21 Spectrofluorometer. A Xe lamp and monochromator were the excitation source, and emitted light was detected by a monochromator and photomultiplier tube. For PLE measurements, the PL intensity at a specific wavelength (380 nm) was measured as a function of excitation wavelength. These PL and PLE measurements were not spatially resolved and therefore give average quantities. To investigate this PL emission with submicron resolution, a PL map was generated with a Klar Mini Pro UV microscope equipped with a 355 nm CW laser and Ocean Insight Maya2000 Pro spectrometer.

¹Klar Scientific, 1615 NE Eastgate Blvd., Unit G, Ste. 3E, Pullman, WA 99163-5300, USA. ²Department of Physics and Astronomy, Washington State University, Pullman, WA 99164-2814, USA. ³Department of Physics, Bowling Green State University, Bowling Green, OH 43403, USA. ✉email: mattmcc@wsu.edu

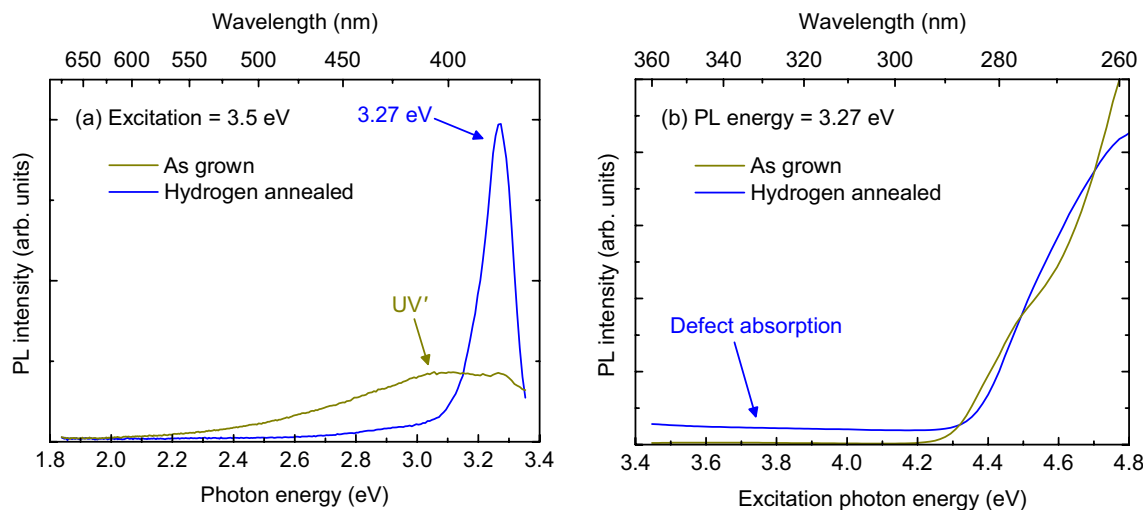


Figure 1. (a) Room temperature PL spectrum of as-grown and hydrogen-annealed Ga_2O_3 under 355 nm (3.5 eV) excitation. The 3.27 eV peak and UV' band are indicated. (b) PLE spectrum of the PL intensity at 380 nm as a function of excitation photon energy. The sub-bandgap defect absorption, which gives rise to the 380 nm (3.27 eV) peak, is indicated.

Results

PL spectra with 355 nm (3.5 eV) excitation are shown in Fig. 1a for the reference and hydrogenated sample. The reference sample shows the UV' band at 400 nm. A smaller peak is observed at 380 nm (3.27 eV). Because this peak occurs well below the UV band, it is attributed to a defect. In the hydrogen-annealed sample, the 3.27 eV peak is large and clearly dominant. From this we conclude that hydrogenation increases the density of the defects responsible for the 3.27 eV peak.

Additional insight can be gleaned from the PLE spectrum for 3.27 eV photon emission (Fig. 1b). For the reference sample, the major contribution to the PL intensity comes from the UV' band. The PLE spectrum shows an absorption onset at 4.4 eV, slightly below the bandgap of 4.5 eV observed with optical transmission spectroscopy. At excitations > 4.7 eV, the PLE increases due to growth in the UV band. Below the bandgap, the PLE intensity is very low.

The hydrogenated sample also has a PLE onset due to the UV' band, although the exact PLE profile is slightly different than the as-grown sample. The PLE spectrum does not show an increase from the UV band at photon energies above the bandgap, presumably because defects compete with the intrinsic PL. The disappearance of the shoulder at ~ 4.4 eV may be due to hydrogen passivation of defects.

Importantly, the hydrogenated sample shows significant PLE intensity *below* the bandgap. The shape of the 3.27 eV PL peak does not depend on the excitation photon energy. The sub-bandgap signal arises from the defect that absorbs photon energies > 3.4 eV and then emits at 3.27 eV. Due to experimental limitations, we could not examine the PLE spectrum < 3.4 eV. Therefore, the difference between the emission peak and absorption threshold (Stokes shift) is < 0.13 eV.

We now turn to the spatial distribution of the 3.27 eV emission. The hydrogen-annealed sample was mapped at a spatial resolution of 700 nm, for a total of 1.8×10^7 spatial (x, y) points, while the reference was mapped at a spatial resolution of 600 nm for a total of 2.7×10^6 points. The integration time was 10 ms per point. The 3.27 eV peak was fit using a bi-Gaussian function using GPU acceleration.

For the reference sample, the PL intensity was essentially zero except for a few distinct spots (Fig. 2). These localized emission centers showed the characteristic defect emission at 3.27 eV. The hydrogenated sample had a much higher areal density of UV emitters, consistent with the spatially averaged PL/PLE results. Figure 3 shows a PL map of the entire hydrogenated sample. Here, weak defect emission was observed everywhere, but especially bright regions were detected as well. The 3.27 eV peak in the spatially averaged spectrum (Fig. 1a) is primarily due to these localized emission centers.

To see where these bright emitters come from, we took a scanning electron microscope (SEM) image and compared it to the PL map of the same area (Fig. 4). The SEM image shows surface pits that were caused by hydrogenation. The long axes of the surface pits are aligned along the c direction. As shown in Fig. 4, there is a clear correlation between the surface defects and defect emission intensity.

Some emitters are so bright, low laser power (< 0.6 mW delivered to the sample) and short integration times (10 ms) had to be used to avoid saturating the spectrometer. The PL intensity versus laser power was linear over the measured range (Supplementary Fig. S3). To obtain a useful benchmark comparison, we collected PL maps of hydrogenated Ga_2O_3 and hydrothermal bulk ZnO under the same experimental conditions. The similarity between the emission energies of these two materials facilitated the comparison. Both samples showed near-UV peaks and no other peaks down to 700 nm (Fig. 5). The lack of defect peaks in ZnO (e.g., the yellow Li-related band^{30,31}) is due to the high excitation laser intensity, which increases the quantum efficiency of the near-UV emission at the expense of defect emission³².

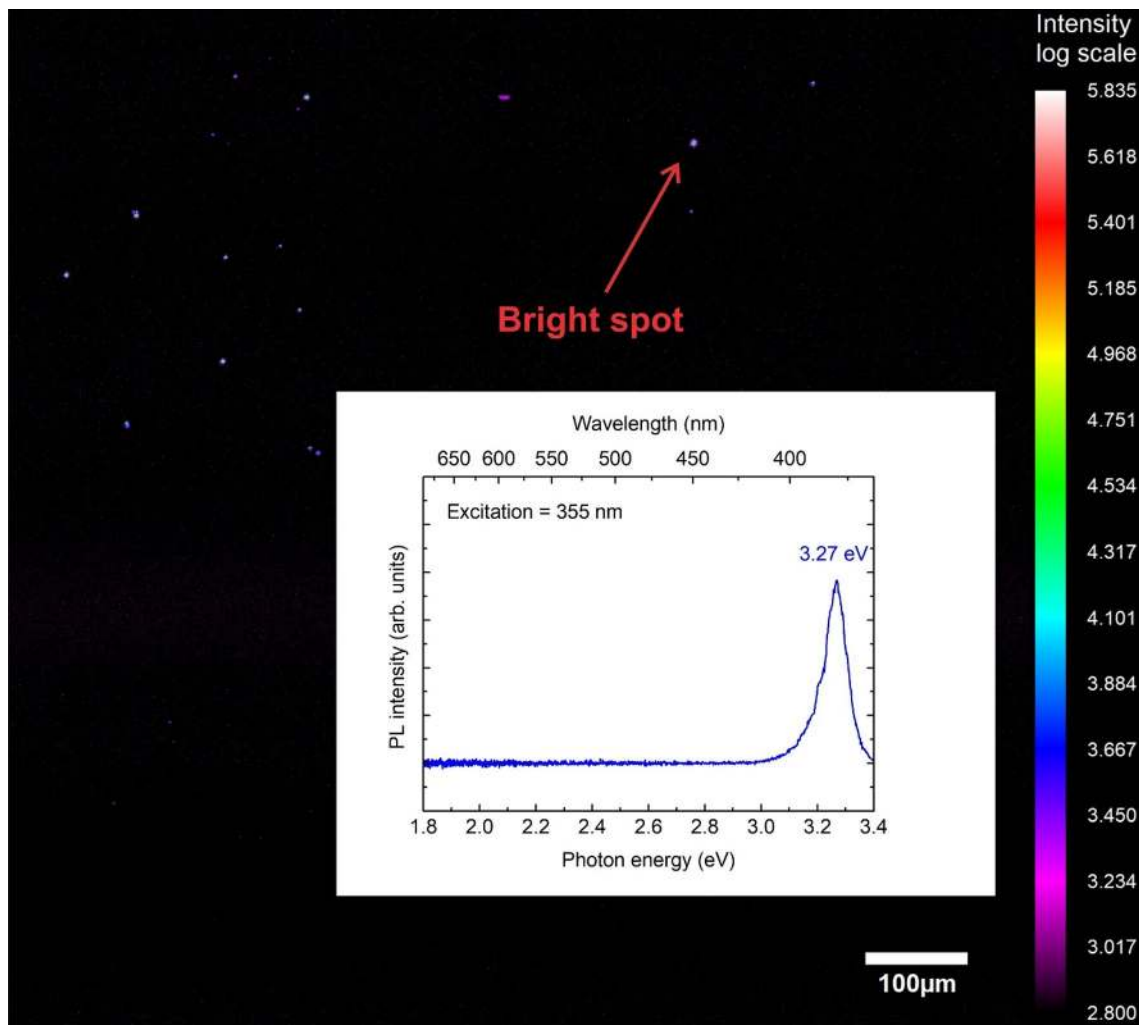


Figure 2. Map of the PL intensity of the 3.27 eV peak for the reference Ga₂O₃ sample. Inset: PL spectrum of one of the bright spots.

Figure 4 shows that the Ga₂O₃ emitters have an intensity *50 times* that of ZnO. Prior work measured an external quantum efficiency of 0.5% for bulk ZnO at room temperature and low excitation intensities (5 W/cm²)³³. Assuming the 50:1 ratio applies at low excitation power, the quantum efficiency of the Ga₂O₃ emitters is ~25%. This relatively high value is consistent with the lack of an observed Stokes shift, which suggests a transition that does not involve significant lattice relaxation³⁴. For example, an electron may transition from the valence band to a defect level. If the defect does not relax, then energy is conserved by phonon emission by the hole. After the hole reaches the top of the valence band, the electron and hole recombine, creating a photon.

What is the identity of these bright, localized emitters? Prior work has shown that hydrogen diffuses into Ga₂O₃ and increases its conductivity³⁵. Annealing in a reducing atmosphere such as hydrogen also decomposes the surface and may result in Ga-rich pits. Elemental mapping of the pits does show evidence that the pits have an excess of Ga and also Si (Supplementary Fig. S4). It is plausible that the pits have a high population of surface or near-surface defects, which emit at 3.27 eV. Alternatively, the pit surfaces may have “intrinsic” surface states that result in the 3.27 eV peak. Regardless of their microscopic structure, these centers are strongly correlated with the surface pits. It is conceivable that these pits act as cavities that enhance the PL intensity.

Conclusions

In conclusion, bright, localized near-UV (3.27 eV at room temperature) emission was observed on the surface of Ga₂O₃. The emission centers show efficient PL emission when excited by photons with energies above 3.4 eV. The brightness of these emitters is remarkable given the generally weak luminescence observed in this material. The strongest emission occurs near surface pits, which are created by annealing in hydrogen. We note that typical PL measurements average over a large spatial region. The results of this study provide a compelling case that one cannot assume that emission centers are distributed homogeneously throughout Ga₂O₃. Rather, the bright emission centers observed here occur only at specific, localized regions on the surface. These localized emitters are reminiscent of those found in 2D semiconductors³⁶, which also involve defects that have not been

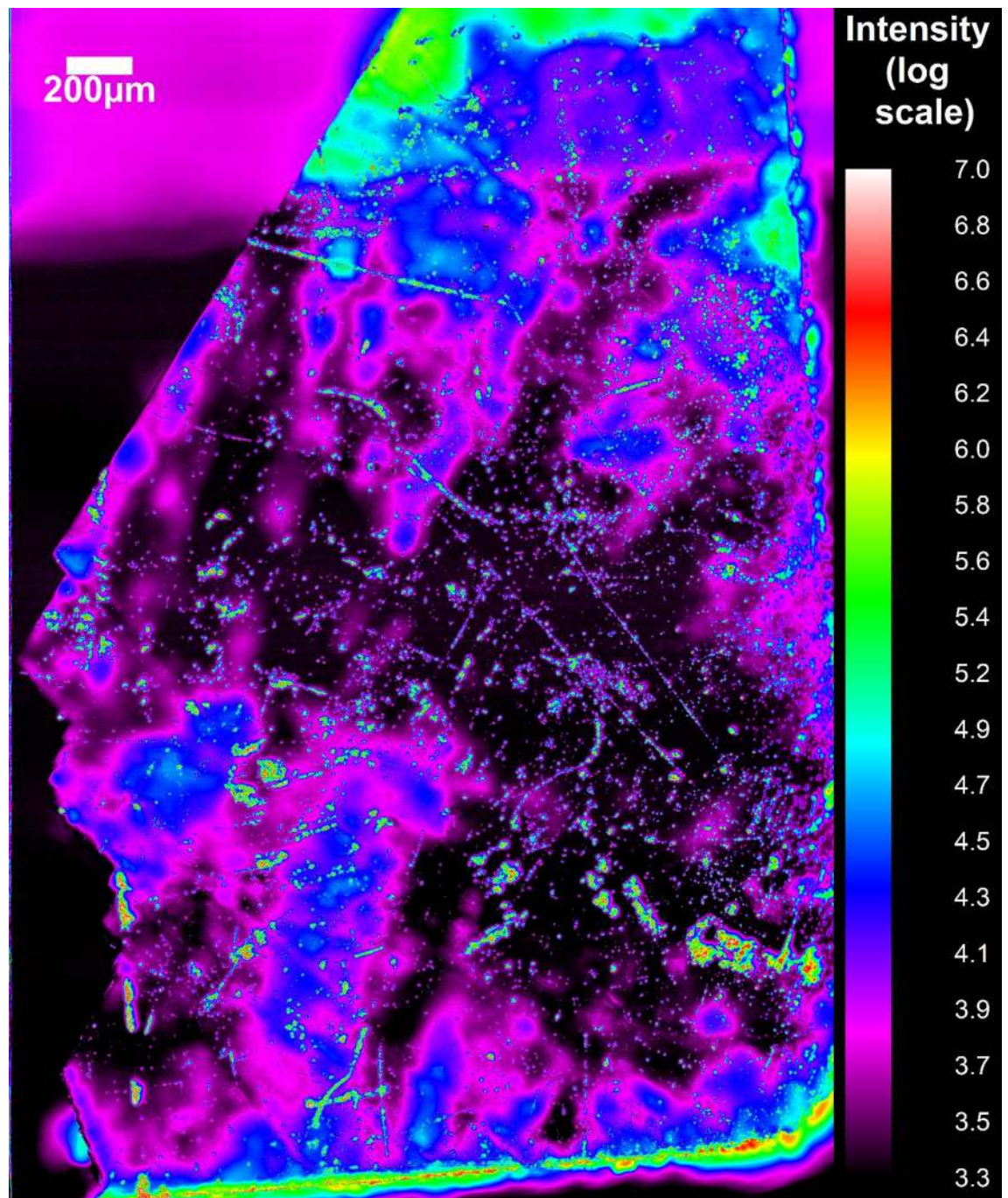


Figure 3. Map of the PL intensity of the 3.27 eV peak for the hydrogenated Ga₂O₃ sample.

positively identified. Future research will improve knowledge of such centers and potentially harness them for optoelectronic or quantum technologies.

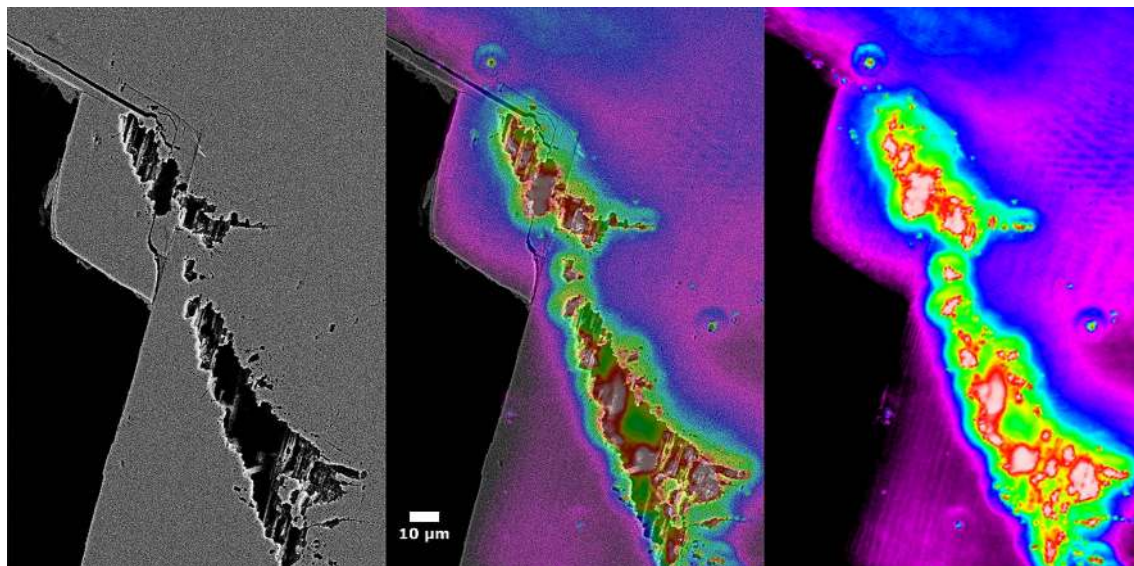


Figure 4. SEM image (left) and map of the 3.27 eV PL intensity (right). An overlaid image is in the center. The defect emission intensity strongly correlates with the surface pits.

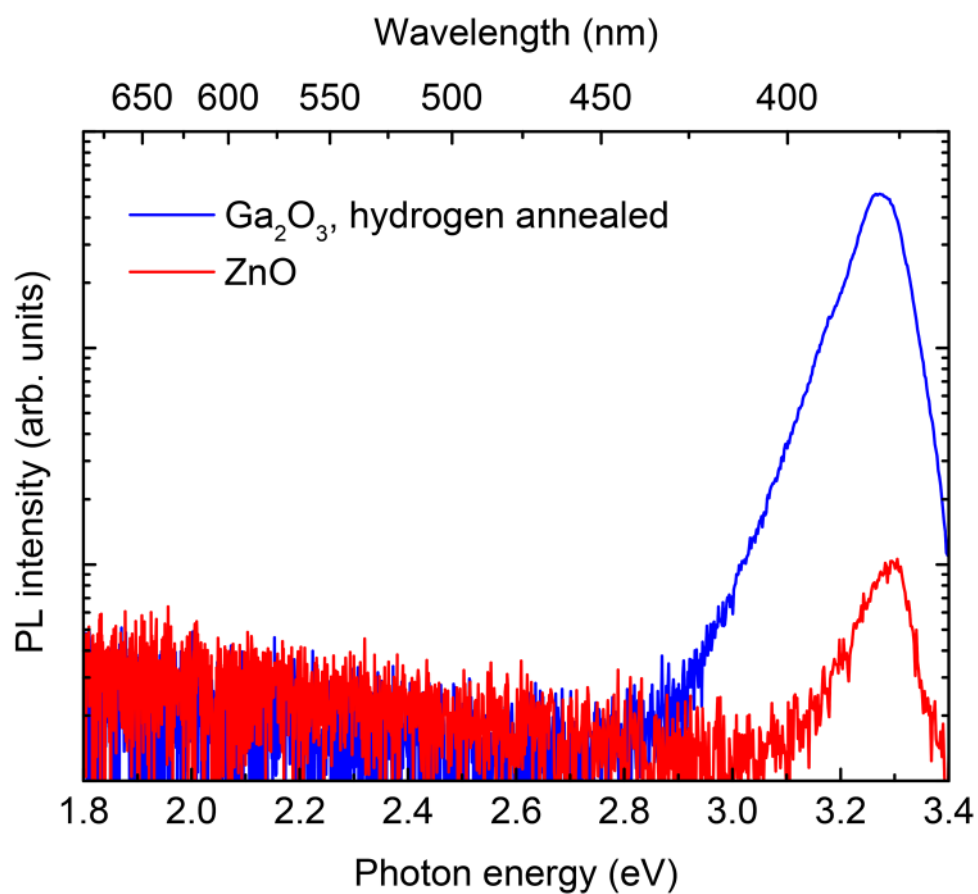


Figure 5. PL spectra (log scale) from an emitter on the surface of hydrogen-annealed Ga₂O₃, and bulk ZnO. The experimental conditions were 1 mW laser power and 10 ms integration time. The PL peak height for Ga₂O₃ is approximately 50 times that of ZnO.

Received: 2 July 2020; Accepted: 30 September 2020

Published online: 03 December 2020

References

- Higashiwaki, M., Sasaki, K., Kuramata, A., Masui, T. & Yamakoshi, S. Development of gallium oxide power devices. *Phys. Status Solidi A* **211**, 21–26 (2014).
- Stepanov, S. I., Nikolaev, V. I., Bougrov, V. E. & Romanov, A. E. Gallium oxide: properties and applications: a review. *Rev. Adv. Mater. Sci.* **44**, 63–86 (2016).
- Pearnton, S. J. *et al.* A review of Ga₂O₃ materials, processing, and devices. *Appl. Phys. Rev.* **5**(011301), 1–56 (2018).
- Pearnton, S. J., Ren, F., Tadjer, M. & Kim, J. Perspective: Ga₂O₃ for ultra-high power rectifiers and MOSFETS. *J. Appl. Phys.* **124**(220901), 1–19 (2018).
- Galazka, Z. β -Ga₂O₃ for wide-bandgap electronics and optoelectronics. *Semicond. Sci. Technol.* **33**(113001), 1–61 (2018).
- Pearnton, S. *et al.* (eds) *Gallium Oxide: Technology, Devices, and Applications* (Elsevier, Amsterdam, 2019).
- Geller, S. Crystal structure of β -Ga₂O₃. *J. Chem. Phys.* **33**, 676–684 (1960).
- Ahman, J., Svensson, G. & Albertsson, J. A reinvestigation of β -gallium oxide. *Acta Crystal. C* **52**, 13361338 (1996).
- McCluskey, M. D. Point defects in Ga₂O₃. *J. Appl. Phys.* **127**(101101), 1–13 (2020).
- He, H. Y. *et al.* First-principles study of the structural, electronic, and optical properties of Ga₂O₃ in its monoclinic and hexagonal phases. *Phys. Rev. B* **74**(195123), 1–8 (2006).
- Peelaers, H. & Van de Walle, C. G. Brillouin zone and band structure of β -Ga₂O₃. *Phys. Status Solidi B* **252**, 828–832 (2015).
- Ratnaparkhe, A. & Lambrecht, W. R. L. Quasiparticle self-consistent GW band structure of β -Ga₂O₃ and the anisotropy of the absorption onset. *Appl. Phys. Lett.* **110**(132103), 1–3 (2017).
- Varley, J. B., Janotti, A., Franchini, C. & Van de Walle, C. G. Role of self-trapping in luminescence and p-type conductivity of wide-band-gap oxides. *Phys. Rev. B* **85**, 081109 (2012).
- Deák, P. *et al.* Choosing the correct hybrid for defect calculations: A case study on intrinsic carrier trapping in β -Ga₂O₃. *Phys. Rev. B* **95**(075208), 1–11 (2017).
- Kananen, B. E. *et al.* Self-trapped holes in β -Ga₂O₃ crystals. *J. Appl. Phys.* **122**(215703), 1–6 (2017).
- Yamaoka, S., Furukawa, Y. & Nakayama, M. Initial process of photoluminescence dynamics of self-trapped excitons in a β -Ga₂O₃ single crystal. *Phys. Rev. B* **95**(094304), 1–5 (2017).
- Wang, Y. S. *et al.* Incident wavelength and polarization dependence of spectral shifts in β -Ga₂O₃ UV photoluminescence. *Sci. Rep.* **8**, 18075 (2018).
- Marcinkevicius, S. & Speck, J. S. Ultrafast dynamics of hole self-localization in β -Ga₂O₃. *Appl. Phys. Lett.* **116**(132101), 1–4 (2020).
- Gao, H. T. *et al.* Optical signatures of deep level defects in Ga₂O₃. *Appl. Phys. Lett.* **112**(242102), 1–5 (2018).
- Binet, L. & Gourier, D. Origin of the blue luminescence of β -Ga₂O₃. *J. Phys. Chem. Solids* **59**, 1241–1249 (1998).
- Huynh, T. T., Lem, L. L. C., Kuramata, A., Phillips, M. R. & Ton-That, C. Kinetics of charge carrier recombination in β -Ga₂O₃ crystals. *Phys. Rev. Mater.* **2**(105203), 1–6 (2018).
- Onuma, T. *et al.* Correlation between blue luminescence intensity and resistivity in β -Ga₂O₃ single crystals. *Appl. Phys. Lett.* **103**(041910), 1–3 (2013).
- Onuma, T. *et al.* Modeling and interpretation of UV and blue luminescence intensity in β -Ga₂O₃ by silicon and nitrogen doping. *J. Appl. Phys.* **124**(075103), 1–6 (2018).
- Villora, E. G. *et al.* Optical Spectroscopy Study on β -Ga₂O₃. *Jpn. J. Appl. Phys. Part 2* **41**, L622–L625 (2002).
- Weiser, P., Stavola, M., Fowler, W. B., Qin, Y. & Pearnton, S. Structure and vibrational properties of the dominant O-H center in β -Ga₂O₃. *Appl. Phys. Lett.* **112**(232104), 1–5 (2018).
- Ritter, J. R. *et al.* Compensation and hydrogen passivation of magnesium acceptors in β -Ga₂O₃. *Appl. Phys. Lett.* **113**(052101), 1–5 (2018).
- Ritter, J. R., Lynn, K. G. & McCluskey, M. D. Hydrogen passivation of calcium and magnesium doped β -Ga₂O₃. *Proc. SPIE* **10919**(109190Z), 1–7 (2019).
- Ritter, J. R., Lynn, K. G. & McCluskey, M. D. Iridium-related complexes in Czochralski-grown β -Ga₂O₃. *J. Appl. Phys.* **126**(225705), 1–6 (2019).
- Kim, H. W. & Kim, N. H. Annealing effects on the properties of Ga₂O₃ thin films grown on sapphire by the metal organic chemical vapor deposition. *Appl. Surf. Sci.* **230**, 301–306 (2004).
- McCluskey, M. D. & Jokela, S. J. Defects in ZnO. *J. Appl. Phys.* **106**(071101), 1–13 (2009).
- McCluskey, M. D. *et al.* Acceptors in ZnO. *J. Appl. Phys.* **117**(112802), 1–6 (2015).
- Simmons, J. G., Foreman, J. V., Liu, J. & Everitt, H. O. The dependence of ZnO photoluminescence efficiency on excitation conditions and defect densities. *Appl. Phys. Lett.* **103**(201110), 1–4 (2013).
- Hauser, M. *et al.* Absolute external luminescence quantum efficiency of zinc oxide. *Appl. Phys. Lett.* **92**(211105), 1–3 (2008).
- Alkauskas, A., McCluskey, M. D. & Van de Walle, C. G. Tutorial: Defects in semiconductors—combining experiment and theory. *J. Appl. Phys.* **119**(181101), 1–11 (2016).
- Islam, M. M. *et al.* Chemical manipulation of hydrogen induced high p-type and n-type conductivity in Ga₂O₃. *Sci. Rep.* **10**, 6134 (2020).
- He, Y.-M. *et al.* Single quantum emitters in monolayer semiconductors. *Nat. Nanotechnol.* **10**, 497–502 (2015).

Acknowledgements

We gratefully acknowledge Slade Jokela, Rick Lytel, Violet Poole, and Jacob Ritter for experimental assistance and helpful discussions. Research at WSU was supported by the U.S. Department of Energy, Office of Basic Energy Sciences, Division of Materials Science and Engineering under Award No. DE-FG02-07ER46386. The data that support the findings of this study are available from the corresponding author upon reasonable request.

Author contributions

J.H., M.D.M., and F.S. wrote the manuscript. J.H. and M.D.M. prepared Figs. 1–5 and Supplemental Figs. S3 and S4. YY performed PL/PLE measurements. M.M.I. and F.S. performed hydrogenation and prepared Supplemental Figs. S1–S2. All authors reviewed the manuscript.

Competing interests

JH is an employee of Klar Scientific and MDM owns equity in the company. FS, MMI, and YY declare no competing interests.

Additional information

Supplementary information is available for this paper at <https://doi.org/10.1038/s41598-020-76967-6>.

Correspondence and requests for materials should be addressed to M.D.M.

Reprints and permissions information is available at www.nature.com/reprints.

Publisher's note Springer Nature remains neutral with regard to jurisdictional claims in published maps and institutional affiliations.



Open Access This article is licensed under a Creative Commons Attribution 4.0 International License, which permits use, sharing, adaptation, distribution and reproduction in any medium or format, as long as you give appropriate credit to the original author(s) and the source, provide a link to the Creative Commons licence, and indicate if changes were made. The images or other third party material in this article are included in the article's Creative Commons licence, unless indicated otherwise in a credit line to the material. If material is not included in the article's Creative Commons licence and your intended use is not permitted by statutory regulation or exceeds the permitted use, you will need to obtain permission directly from the copyright holder. To view a copy of this licence, visit <http://creativecommons.org/licenses/by/4.0/>.

© The Author(s) 2020